



## Synthesis and Characteristics of the Magnetic Properties of $\text{Fe}_3\text{O}_4$ -(CTAB-montmorillonite) Composites, based on Variation in $\text{Fe}^{3+}/\text{Fe}^{2+}$ Concentrations

SRI HILMA SIREGAR<sup>1\*</sup>, KARNA WIJAYA<sup>2\*</sup>, EKO SRI KUNARTI<sup>2</sup> and AKHMAD SYOUFIAN<sup>2</sup>

<sup>1</sup>Department of Chemistry, Faculty of Mathematics & Natural Science, University Muhammadiyah Riau, Pekanbaru, Indonesia.

<sup>2</sup>Department of Chemistry, Faculty of Mathematics & Natural Science, Gadjah Mada University, Yogyakarta, 55281, Indonesia.

\*Corresponding author E-mail: karnawijaya@ugm.ac.id, srihilma.s@gmail.com

<http://dx.doi.org/10.13005/ojc/340213>

(Received: January 01, 2018; Accepted: March 01, 2018)

### ABSTRACT

This research aims to determine characteristics of the magnetic properties of  $\text{Fe}_3\text{O}_4$ - (CTAB-Montmorillonite) composites and the effect of variation in  $\text{Fe}^{3+}/\text{Fe}^{2+}$  concentrations on the characteristics of  $\text{Fe}_3\text{O}_4$ - (CTAB-Montmorillonite) composites.  $\text{Fe}_3\text{O}_4$ - (CTAB-Montmorillonite) composites were synthesized using an *in situ* co-precipitation method. The synthesis was carried out by mixing  $\text{FeCl}_3 \cdot 6\text{H}_2\text{O}$  and  $\text{FeSO}_4 \cdot 7\text{H}_2\text{O}$  (in different concentrations) with a mole ratio of  $\text{Fe}^{3+}$  to  $\text{Fe}^{2+}$  by 2:1, which was then mixed into the CTAB-montmorillonite suspension. This mixture was stirred using a magnetic stirrer at 3500 rpm for 30 min. at a temperature of 85 °C, then the ammonia solution 25% was added. reaction lasted for 24 hours. The resulting composites were characterized using XRD, BET, and VSM to measure the magnetic properties of the materials. Results of the XRD data analysis showed that the values of  $d(311)$  is equal to 2.5686 Å and  $d(220)$  is equal to 2.947 Å, which are the characteristics of the materials known as magnetite. Based on the VSM data obtained, the magnetic saturation (Ms) values for samples of different concentrations were as follows: SH01=14.0 emu/g, SH02= 29.0 emu/g, SH03= 28.9 emu/g, SH04= 45.2 emu/g, and SH05= 64.1 emu/g.

**Keywords:** Montmorillonite,  $\text{Fe}_3\text{O}_4$ -(CTAB-Mt), Magnetite.

### INTRODUCTION

In recent years, the application of magnetic composite materials to overcome environmental problems is one problem that has

attracted much attention from researchers. One of the materials currently being developed is magnetite ( $\text{Fe}_3\text{O}_4$ ) which has advantages due to its crystalline properties and its magnetism, making it easier to regenerate<sup>1,2</sup>. Magnetite synthesis in



This is an  Open Access article licensed under a Creative Commons Attribution-NonCommercial-ShareAlike 4.0 International License (<https://creativecommons.org/licenses/by-nc-sa/4.0/>), which permits unrestricted NonCommercial use, distribution and reproduction in any medium, provided the original work is properly cited.

nanometer scale has been done by various methods, such as by ways of sol-gel reactions, chemical solutions, sonochemistry, and co-precipitation<sup>3,4</sup>. Magnetite nanoparticles are materials that have a number of advantages such as superparamagnetism, high magnetic saturation, a good anisotropy contribution, and biocompatibility. In addition to their magnetic properties, magnetic materials can be utilized in various applications such as in photo catalysis, biological applications, biomedicine, metal separation, and absorbents<sup>5,6</sup>.

Various studies have reported that unmodified magnetite nanoparticles have low thermal stability and low water solubility, and may react backward to form FeOOH at the intermediate phases<sup>7</sup>. The main composition of bentonite is mineral montmorillonite which has ion exchange properties. These materials are best used as an adsorbent to adsorb various water contaminants in the liquid waste. The presence of a negative charge in the montmorillonite crystalline interlayer, which is balanced by the presence of cations within its interlayer space, enables the binding of positively charged contaminant species such as organic and inorganic cations of metals<sup>8,9</sup>. The advantages of the use of these materials as an adsorbent are that they have a high surface area, are easy to obtain and not expensive, and have fairly good stability<sup>10</sup>. However, the disadvantage of the use of montmorillonite as an adsorbent is that it forms colloids/suspensions in liquid. This will pose a problem when recollecting montmorillonite particles after absorbing contaminants. In large-scale volumes of waste, separation by filtration and centrifugation takes time and costs a lot<sup>11,12</sup>.

Clay of the smectite class is characterized by octahedral alumina and tetrahedral silicates with a ratio of 2:1. The substitution of Al<sup>3+</sup> in the octahedral sheet with Mg<sup>2+</sup> results in a negative layer charge that is compensated by hydrated cations absorbed in the interlamellar space. These cations can easily be substituted by others presenting in a solution<sup>13</sup>. Pillared interlayered clay includes a new family of clay based on two-dimensional materials and is used in absorption and catalysis. Clay pillaring with inorganic polycations results in the production of thermally stable rigid cross-linked materials with a large surface area, a particular porous texture, and

acidity. The properties of pillared clay are determined by several factors such as preparation conditions of the polycations, the method of intercalation, and washing and drying steps<sup>14</sup>. By utilizing the characteristic properties of montmorillonite, solving the montmorillonite problem as an adsorbent, and modifying montmorillonite by combining the magnetite particles (iron oxides) with montmorillonite, there will be a chance of generating new materials which have two main properties, i.e. cationic exchangers derived from montmorillonite and responses to the external magnetic field due to the presence of magnetite particles in the montmorillonite interlayer. The first property is used to adsorb contaminants while the second one is used to recover the distributed composites in the liquid using permanent magnetic bars.

In this research, the Fe<sub>3</sub>O<sub>4</sub>-(CTAB-Mt) composites were synthesized using the *in situ* co-precipitation method. The research scope was variation in the concentration of the precursors, i.e. Fe<sup>3+</sup> and Fe<sup>2+</sup>, with a mole ratio of 2:1. The manufacture of these composites is intended to improve the quality of the adsorbents so as to simplify the separation process. The Fe<sub>3</sub>O<sub>4</sub>-(CTAB-Mt) composites were characterized by FT-IR, XRD, BET, SEM-Mapping, and VSM.

## MATERIALS AND METHODS

### Materials

CTAB-montmorillonite was derived from the results of previous studies. The chemicals used in this study were FeCl<sub>3</sub>·6H<sub>2</sub>O, FeSO<sub>4</sub>·7H<sub>2</sub>O, NH<sub>4</sub>OH 25% (w/v). All chemicals used were of analytical reagent grade, obtained from the Merck Company. Double-ionized water was used in all experiments.

### Synthesis of Fe<sub>3</sub>O<sub>4</sub>-(CTAB-Mt)

Montmorillonite-CTAB magnetic synthesis was done using the *in situ* co-precipitation method. As many as 5 g of Bentonite-CTAB was dissolved in 500 mL of aquabidest. The solution was stirred for 24 h until it formed a homogeneous suspension. As many as 250 mL of a solution consisting of FeSO<sub>4</sub>·7H<sub>2</sub>O and FeCl<sub>3</sub>·6H<sub>2</sub>O was prepared with variation in the concentrations of Fe<sup>3+</sup> and Fe<sup>2+</sup> and then mixed into a bentonite-CTAB suspension.

Afterwards, they were stirred at 3500 rpm for 30 min. at a temperature of 85 °C. As many as 25 mL of  $\text{NH}_4\text{OH}$  was added slowly to the mixture above until it reached pH 10 to 11 and stirred for 2 h more. The bentonite-CTAB magnetite composites generated were washed using hot aquabidest and then separated using the decantation method using an external magnet. Subsequently, they were dried at a temperature of 80 °C for 3 hours. The results obtained were analyzed using FT-IR to determine the functional group, XRD to determine crystallinity, and BET and VSM to determine the magnetic properties of the materials.

## RESULTS AND DISCUSSIONS

### Synthesis of $\text{Fe}_3\text{O}_4$ -(CTAB-Mt)

The  $\text{Fe}_3\text{O}_4$ -(CTAB-Montmorillonite) composites were synthesized using intercalation of metal polycations and intercalation of agents into the interlayers of CTAB-Mt silicates. CTAB-Mt materials were first synthesized by Siregar<sup>15</sup> in previous studies. These intercalated metal polycations replaced cations, exchanged interlayers, and, with calcination of iron polycations, changed into an oxide that supported the interlayers of CTAB-Mt silicates. Iron oxides enter the space between the sheets of CTAB-Mt through an ion exchange process or are deposited on a negatively charged CTAB-Mt surface. Ions with a higher charge tend to replace ions with a lower charge.  $\text{Fe}^{3+}$  contains more cations in the space between the CTAB-Mt sheets ( $\text{Na}^+$ ,  $\text{K}^+$ ,  $\text{Ca}^{2+}$ , and  $\text{Mg}^{2+}$ ), thus  $\text{Fe}^{3+}$  can replace the cation's cations.  $\text{Fe}^{2+}$  may experience ion exchange or attach to negatively charged CTAB-Mt surfaces.  $\text{Fe}^{3+}$  and  $\text{Fe}^{2+}$  then form  $\text{Fe}(\text{OH})_2$  and  $\text{Fe}(\text{OH})_3$  when  $\text{NH}_4\text{OH}$  is added. After the treatment,  $\text{Fe}(\text{OH})_2$  and  $\text{Fe}(\text{OH})_3$  are hydrated in iron oxides ( $\text{Fe}_3\text{O}_4$ ) to produce composites that have magnetic properties.

Generally, the interpretation of infrared spectra CTAB-Mt and  $\text{Fe}_3\text{O}_4$ -(CTAB-Mt) does not differ significantly (Fig.1). The resulting characteristics show that infrared spectra can hardly provide a clear indication of the presence of iron oxides as a pillar within CTAB-Mt interlayers. The presence of magnetite nanoparticles is indicated by the absorption bands at 586.36 and 462.92  $\text{cm}^{-1}$ .

These bands are attributed to FeO stretches of bulk magnetite and the shifting of the band of the FeO bond of bulk magnetite to a higher wavenumber, respectively. The OH (water-free) stretching vibration band and bending vibration peak appear at 3432.30 and 1635.64  $\text{cm}^{-1}$  in  $\text{Fe}_3\text{O}_4$ -(CTAB-Mt), respectively. These indicate that  $\text{Fe}_3\text{O}_4$  nanoparticles in the montmorillonite interlayer successfully.

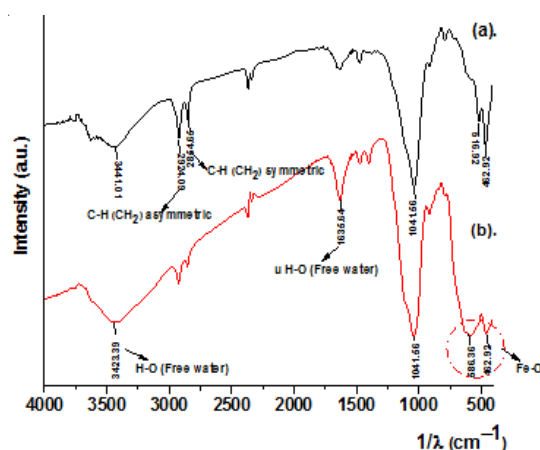


Fig. 1. IR spectra of CTAB-Mt (a) and  $\text{Fe}_3\text{O}_4$ -(CTAB-Mt) (b)

The XRD patterns of CTAB-Mt and  $\text{Fe}_3\text{O}_4$ -(CTAB-Mt) are shown in Fig. 2. Based on the results of previous research<sup>15</sup>, there is a shift in the angle by  $2\theta$  or more to the right (i.e. ranging from 4.61 to 4.96°) as a result of the formation of  $\text{Fe}_3\text{O}_4$  in the intercross of CTAB-Mt silicates, which indicates that the intercalation process is successful. The  $\text{Fe}_3\text{O}_4$ -(CTAB-Mt) composites show wider and less sharp reflections. This happens due to the delamination of the silicates' layer structure because of the intercalation process of complex metal cations. The  $\text{Fe}_3\text{O}_4$ -(CTAB-Mt) composites show additional diffraction peak positions at  $2\theta = 30.0$ , 35.3, 43.0, 53.4, 56.9, and 62.5° corresponding to the (220), (311), (40), (422), (511), and (440) planes of  $\text{Fe}_3\text{O}_4$  in a cubic phase, respectively. It is clear that only the phase of  $\text{Fe}_3\text{O}_4$  is detectable<sup>16</sup>. The  $\text{Fe}_3\text{O}_4$  peaks formed on the XRD curve are of very high intensity, while the peak characteristic of CTAB-Mt is reduced in intensity. This indicates the entry of iron oxides into CTAB-Mt layers. These data show good agreement with the standard data for the  $\text{Fe}_3\text{O}_4$  structure (JCPDS card file No. 3-863).

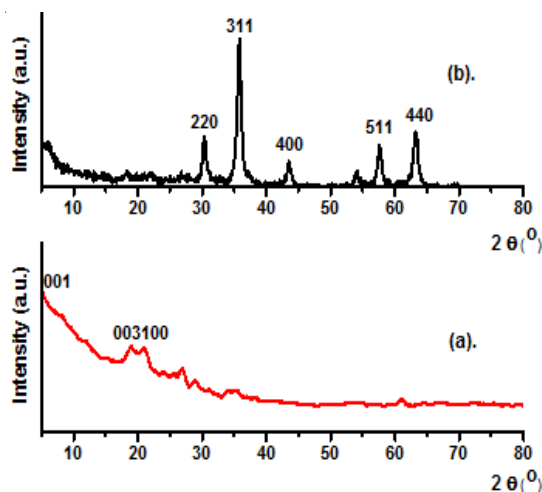


Fig. 2. XRD patterns of CTAB-Mt (a) and  $\text{Fe}_3\text{O}_4$ -(CTAB-Mt) (b)

The typical SEM images of CTAB-Mt and  $\text{Fe}_3\text{O}_4$ -(CTAB-Mt) are demonstrated in Fig. 3. Very fine microparticles can be observed with a diameter of 0.1  $\mu\text{m}$  in the SEM of  $\text{Fe}_3\text{O}_4$ -(CTAB-Mt) composites. The presence of these fine particles leads to an increase in the porosity and the surface area of the modified CTAB-Mt. It can be seen from this figure that CTAB-Mt has large particles and a smooth non-porous surface (Fig. 3a), but after intercalation by polymeric inorganic cations, those particles become loose and there are more stripped, loose, and curly sliced layers. The image shows the regular crystal structure and even distribution of diameters found in synthesized  $\text{Fe}_3\text{O}_4$  nanoparticles. The micrographs of composite materials have a lot of particles covered, which suggest the presence of synthesized  $\text{Fe}_3\text{O}_4$  particles covering the surfaces of Mt<sup>17</sup>.

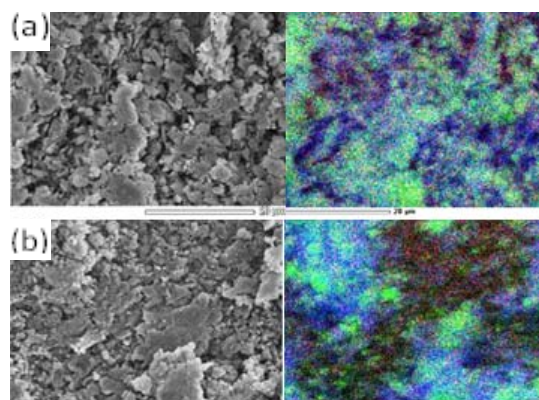


Fig. 3. SEM images and iron mapping of CTAB-Mt (a) and  $\text{Fe}_3\text{O}_4$ -(CTAB-Mt) (b)

The EDX analysis of the prepared adsorbents was carried out to determine their elemental compositions. Table 1 shows the EDX spectrum and elemental compositions of CTAB-Mt and  $\text{Fe}_3\text{O}_4$ -(CTAB-Mt). The EDX spectrum of CTAB-Mt shows that the percentages of the mass of MgO,  $\text{Al}_2\text{O}_3$ , and  $\text{SiO}_2$  (i.e. by 2.19, 13.64, and 54.59 respectively) were the highest, while other elements like FeO were present in minute quantities (2.85 %). The EDX spectrum of  $\text{Fe}_3\text{O}_4$ -(CTAB-Mt) shows the highest percentage of the mass of FeO (37.09) coupled with minute quantities of MgO,  $\text{Al}_2\text{O}_3$ ,  $\text{SiO}_2$  (i.e. by 1.04, 6.05, and 24.73 respectively). The highest percentage of iron in the EDX spectrum of  $\text{Fe}_3\text{O}_4$ -(CTAB-Mt) resulted from magnetic nanoparticles. Thus the EDX spectrum of  $\text{Fe}_3\text{O}_4$ -(CTAB-Mt) confirms that CTAB-Mt was successfully loaded by magnetite nanoparticles<sup>18</sup>. Consequently, the FeO mapping of  $\text{Fe}_3\text{O}_4$ -(CTAB-Mt) clearly indicates good distribution of magnetite (blue dot) in  $\text{Fe}_3\text{O}_4$ -(CTAB-Mt) (Fig. 3b).

Table 1: Elemental composition of CTAB-Mt and  $\text{Fe}_3\text{O}_4$ -(CTAB-Mt) samples determined by EDX

Samples	Element	Mass %	Compound	Mass %
CTAB-Mt	Mg	1.32	MgO	2.19
	Al	7.22	$\text{Al}_2\text{O}_3$	13.64
	Si	25.52	$\text{SiO}_2$	54.59
	K	1.12	$\text{K}_2\text{O}$	1.35
	Ca	0.89	CaO	1.25
	Fe	2.22	FeO	2.85
$\text{Fe}_3\text{O}_4$ -(CTAB-Mt)	Mg	0.63	MgO	1.04
	Al	3.20	$\text{Al}_2\text{O}_3$	6.05
	Si	11.56	$\text{SiO}_2$	24.73
	S	0.96	$\text{SO}_3$	2.4
	K	0.55	$\text{K}_2\text{O}$	0.66
	Fe	28.83	FeO	37.09

**The characteristics of the structure and components of  $\text{Fe}_3\text{O}_4$ -(CTAB-Mt) based on variation in the concentration of its precursors.**

Results of the XRD pattern analysis for  $\text{Fe}_3\text{O}_4$ -(CTAB-montmorillonite) composites on variation in the precursor concentration can be seen in Fig. 4. Based on the XRD pattern of  $\text{Fe}_3\text{O}_4$ , it is indicated that iron oxides are composed of spinel structures whose characteristic peaks occur at  $2\theta$ ,  $30,32^\circ$  (200),  $35,82^\circ$  (311),  $42,90^\circ$  (400),  $54,18^\circ$  (422),  $56,98^\circ$  (511), and  $62,98^\circ$  (440) and are appropriate for standard cards (Ref Code  $\text{Fe}_3\text{O}_4$ : 96-900-5840). Based on the XRD spectrum pattern, it can be concluded that if the concentration is higher, then the peak intensity typical of  $\text{Fe}_3\text{O}_4$  will also be higher. For example, in the precursor concentration of  $(\text{Fe}^{2+}/\text{Fe}^{3+})$  0.025: 0.5 mg/L, the peak intensity at 311 is 65, while in a high concentration of 0.2: 0.4 mg/L, the peak intensity at 311 is 197. The  $\text{Fe}_3\text{O}_4$  composites prepared with a precursor concentration of 0.1: 0.2 mg/L (SH04) and 0.2: 0.4 mg/L (SH05), except for composites with lower precursor concentrations such as samples SH04 and SH05, have the peaks at the same diffraction angle as  $\text{Fe}_3\text{O}_4$  nanoparticles (JCPDS). If  $\text{Fe}_3\text{O}_4$  is a nanoparticle, it forms magnetite which is successfully combined with montmorillonite and the resulting composites produce a magnet. This was evidenced by bringing the composites closer to the magnetic field, the composites that have magnetic properties will stick to the magnet. Based on this simple magnetism test, it is revealed that there were three composites that had magnetic properties, i.e. Composites in the samples SH04 and SH05. While composites in the samples SH03, SH01, and SH02 showed very weak magnetic properties.

The similarity between samples SH04 and SH05 with  $\text{Fe}_3\text{O}_4$  nanoparticles is evident in Fig. 4 through a straight line connecting the peaks of the diffraction results. This indicates that samples SH04 and SH05 contain magnetite. The peaks in other composite diffraction patterns are less strong compared to those of composites in the samples SH04 and SH05.

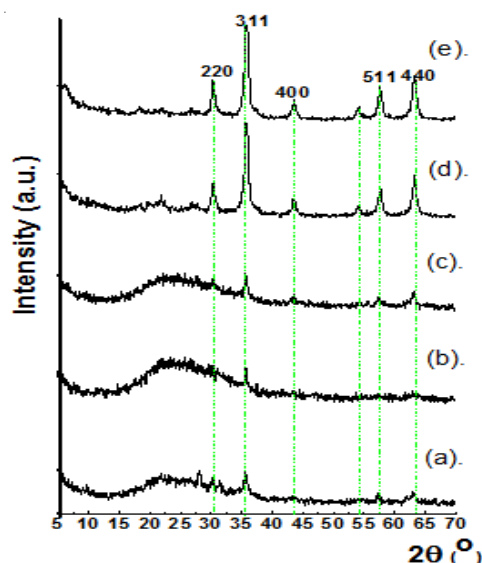


Fig. 4. The XRD analysis of Samples SH02 (a), SH01 (b), SH03(c), SH04 (d), and SH05 (e)

The  $\text{N}_2$  adsorption-desorption of the  $\text{Fe}_3\text{O}_4$ -(CTAB-Mt) composite desorption, as determined in type IV and hysteresis loop of this isotherm type, was H3 in the classification of IUPAC, as shown in Fig. 5, and this clearly indicates that  $\text{Fe}_3\text{O}_4$ -(CTAB-Mt) represents a mesoporous feature. According to Fig. 5, the specific surface area, the total pore volume, and the average pore diameter were obtained and shown in Table 2. Composites showed significant increases in terms of their BET surface area, pore volume, and average size compared with CTAB-Mt and the success of  $\text{Fe}_3\text{O}_4$ -(CTAB-Mt) was evident from increased interlayer spacing<sup>19</sup>. The majority of the pores were macropores for the CTAB-Mt and mesoporous for  $\text{Fe}_3\text{O}_4$ -(CTAB-Mt). Based on Table 2, the BET surface area of CTAB-Mt was  $0.000 \text{ m}^2/\text{g}$ , as proposed by Parolo *et al.*,<sup>20</sup> in organoclays with a surfactant loading exceeding 1.5 CEC of bentonite, the molecules are highly intercalated in the clay mineral interlayer space as well as in the interparticle pores, which leads to a decreased surface area and pore volume. Hence, the clay layers are almost completely enclosed and the pores are enlarged by the loaded surfactant molecules. This is consistent with the report of Kiransan *et al.*,<sup>21</sup> that a value greater than 1.0 will reduce the increase of d-spacing. This is probably due to an excessive surfactant concentration, which causes the surfactant to be arranged laterally in a

monolayer in bentonite. The average pore diameter of CTAB-Mt decreased slightly and most pore diameter ranged from 19.010 to 21.00Å. However, after modification with Fe<sub>3</sub>O<sub>4</sub>, the mesopore volume decreased evidently and there was an increase in the proportion of pore diameters. Thus, the enlargement of the BET surface area could be mainly attributed to the increase in the pore diameter and the BET surface area in the proportion of smaller mesopores.

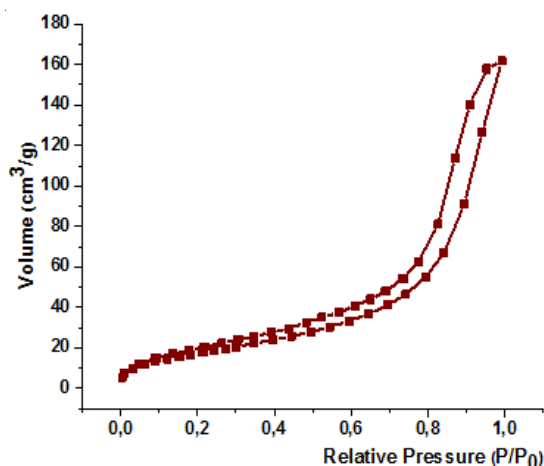


Fig. 5. The N<sub>2</sub> adsorption-desorption curve of Fe<sub>3</sub>O<sub>4</sub>-(CTAB-Mt)

Table 2: The BET surface area and micropore structure parameters

Samples	BET surface (m <sup>2</sup> /g)	Average Poe diameter (Å)	Total pore volume (cm <sup>3</sup> /g)
CTAB-Mt	0.000	19.01	0.874
Fe <sub>3</sub> O <sub>4</sub> -(CTAB-Mt)	64.806	46.596	0.247

Measurement using VSM was done by giving a magnetic field up to 1 Tesla. The magnetic moment generated by the sample as a result of the addition of a magnetic field signifies the magnetic properties of the materials. The greater the magnetic moment of a material is, the greater of the magnetic. The analysis of magnetic properties was carried out using a VSM (Vibrating Sample Magnetometer), particularly Oxford VSM 1.2H and it was undertaken in the Magnetic-Composite Materials-PTBIN-BATAN

field. The magnetic hysteresis cycles of composites are shown in Fig. 6. The magnetic hysteresis cycle of Fe<sub>3</sub>O<sub>4</sub>-(CTAB-Mt) composite properties belongs to a soft magnet because the hysteresis cycle has a backward sequence which is almost symmetric when subjected to a magnetic field or when a magnetic field is removed. The data and coerciveness (Hc) are shown in Table 3 sample A SH05B = SH04, C=SH3, D-SH01 and E= SH02 . It can be concluded that precursor concentrations greatly affect the magnetic properties of the composites. The higher the precursor concentration is, the higher the magnetic properties of the composites are.

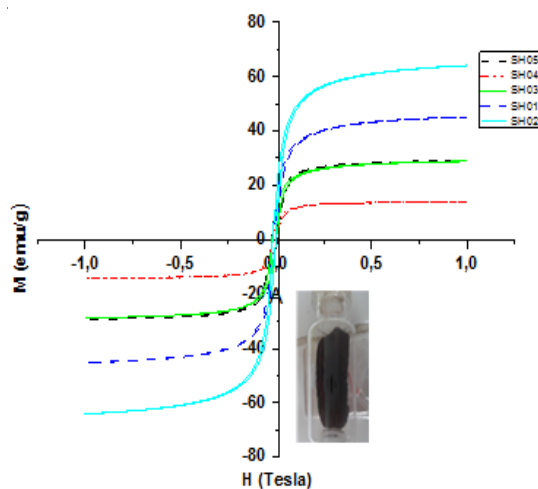


Fig. 6. Magnetization curves of Samples SH05 (a), SH04 (b), SH03 (c), SH01 (d), and SH02 (e) with variation in the concentration of precursors (Fe<sup>2+</sup>/Fe<sup>3+</sup>).

Table 3: Dependence of Ms, Mc, and Hc on the content of Fe<sub>3</sub>O<sub>4</sub> in Fe<sub>3</sub>O<sub>4</sub>-(CTAB-Mt)

Samples	Mr (emu/g)	Ms (emu/g)	Hc (Tesla)
Sample SH05	17.9	64.1	0.0161
Sample SH04	11	45.2	0.0198
Sample SH03	9.12	28.9	0.0191
Sample SH01	9.83	14	0.0194
Sample SH02	4.93	29	0.0259

## CONCLUSION

The Fe<sub>3</sub>O<sub>4</sub>-(CTAB-Mt) composites have been synthesized using the *in situ* co-precipitation

method and characterized by XRD, BET, VSM, and SEM-EDX-mapping. Based on the research findings, the resulting Fe<sub>3</sub>O<sub>4</sub>-(CTAB-Mt) composites are blackish brown in color and have strong magnetic properties. The best characters of the composite are obtained from the ration of precursor concentrations (Fe<sup>2+</sup>/Fe<sup>3+</sup>) by 0.2: 0.4 mg/L. The greater the variation in the concentration of the precursors in the manufacture of Fe<sub>3</sub>O<sub>4</sub>-(CTAB-Mt)

composites is, the higher the value of the resulting coercive field (H<sub>c</sub>) is, thus the magnetic properties will also be greater.

#### ACKNOWLEDGMENT

The Authors are grateful to UMRI & UGM for admission and facilities to conduct the research, and Kemenristek DIKTI Grant for financial support through Penelitian Disertasi Doktor 2018.

#### REFERENCES

- Masindi, V.; Gitari, M.W.; Tutu, H.; De-Beer, M. *J. Water Process Eng.*, **2017**, *15*, 2-17.
- Lou, Z.; Zhou, Z.; Zhang, W.; Zhang, X.; Hu, X.; Liu, P.; Zhang, H. *J. Taiwan Chem. Eng.*, **2015**, *49*, 199-205.
- Wan, D.; Li, W.; Wang, G.; Chen, K.; Lu, L.; Hu, Q. *Appl. Surf. Sci.*, **2015**, *349*, 988-996.
- Guz, L.; Curutchet, G.; Sanchez, R.M.T.; Candal, R.; *J. Environ. Chem. Eng.*, **2014**, *2*, 2344-2351.
- Chen, D.; Li, W.; Wu, Y.; Zhu, Q.; Lu, Z.; Du, G.; *J. Chem. Eng.*, **2013**, *221*, 8-15.
- Hao, X.; Liu, H.; Zhang, G.; Zou, H.; Zhang, Y.; Zhou, M.; Gu, Y. *Appl. Clay Sci.*, **2012**, *55*, 177-180.
- Chen, H.; Li, Y.; Wang, S.; Zhou, Y. *Appl. Surf. Sci.*, **2017**, *402*, 384-391.
- Chang, J.; Ma, J.; Ma, Q.; Zhang, D.; Qiao, N.; Hu, M.; Ma, H.; *Appl. Clay Sci.*, **2016**, *110*, 132-140.
- Wu, H.; Xie, H.; He, G.; Guan, Y.; Zhang, Y. *Appl. Clay Sci.*, **2016**, *119*, 161-169.
- Yan, L.; Li, S.; Yu, H.; Shan, R.; Du, B.; Liu, T. *Powder Technol.*, **2016**, *301*, 632-640.
- Lv, G.; Li, Z.; Jiang, W. T.; Chang, P. H.; Liao, L. *Mater. Chem. Phys.*, **2015**, *162*, 417- 424.
- Lian, L.; Cao, X.; Wu, Y.; Sun, D.; Lou, D. *Appl. Surf. Sci.*, **2014**, *289*, 245-251.
- Fatimah, I.; Narsito, Karna, W.; *Indo. J. Chem.* **2009**, *9*, 1, 16-12.
- Suseno, A.; Wijaya, K.; Trisunaryanti, W.; Roto, Priyono. *Int. J. Chem. Tech. Res.*, **2017**, *10*, 2, 40-44.
- Siregar, S.H.; Wijaya, K.; Kunarti, E.S.; Syoufian, A.; Suyanta. *Asian J. Chem.*, **2018**, *30*(1) 25-28.
- Wu, L.; Ye, Y.; Liu, F.; Tan, C.; Liu, H.; Wang, S.; Wang, J.; Yi, W.; Wu, W. *Appl. Clay Sci.*, **2013**, 83-84, 405-414.
- Martins, M.G.; Martins, D.O.T.A.; de Carvalho, B. L.C.; Mercante, L.A.; Soriano, S.; Andruh, M.; Vieira, M. D.; Vaz, M.G.F. *J. Solid State Chem.*, **2015**, *228*, 99-104.
- Ishaq, M.; Sultan, S.; Ahmad, I.; Ullah, H.; Yaseen, M.; Amir, A. *J. Saudi Chem. Soc.*, **2016**, *21*(2) 43-151.
- Zhang, H.; Liang, X.; Yang, C.; Niu, C.; Wang, J.; Su, X.; *J. Alloys Compd.*, **2016**, *688*, 1019-1027.
- Parolo, M. E.; Pettinari, G. R.; Musso, T.B.; María P. Sánchez-Izquierdo, Fernández, L.G. *Appl. Surf. Sci.*, **2014**, *320*, 356–363.
- Kiransan, M.; Soltani, R.D.C.; Hassani, A.; Karaca, S. *J. Taiwan. Inst. Chem. Eng.*, **2014**, *45*, 2565-2577.